Scientia Iranica B (2011) 18 (5), 1116–1125

Sharif University of Technology

Scientia Iranica

Transactions B: Mechanical Engineering

www.sciencedirect.com

Frequency response of atomic force microscopy microcantilevers oscillating in a viscous liquid: A comparison of various methods

M.H. Korayem *, **N. Ebrahimi**, **M.S. Sotoudegan**

Robotic Research Laboratory, Center of Excellence in Experimental Solid Mechanics and Dynamics, School of Mechanical Engineering, Iran University of Science and Technology, Tehran, P.O. Box 18846, Iran

Received 24 December 2010; revised 12 May 2011; accepted 27 June 2011

KEYWORDS

Atomic force microscopy;
Tapping mode;
Viscous fluid;
Resonance frequencies;
Hydrodynamic effects.

Abstract Operating an Atomic Force Microscopy (AFM) with the cantilever and sample immersed in a liquid has many advantages, including the elimination of capillary forces and reduction of van der Waals forces in the study of liquid–solid interactions. Accurately identifying the maximum of the amplitude–frequency curves at which resonances occur is a challenging issue. The frequency response of a cantilever beam in a viscous liquid near a surface depends on the hydrodynamic loadings. First, in this paper, there is a comparison of predicted resonant frequencies from five different theoretical models, with measurements for the case of an ambient liquid of infinite extent. The precision of each method is indicated. Then, the motion of microcantilevers of variable widths close to a solid surface is simulated. When the cantilever tip approaches the sample surface gradually, the effect of squeezed film damping causes the resonance frequencies to shift toward lower values at lower amplitudes, and subsequently as the tip-sample separation becomes smaller, the resonance peaks seem to vanish completely. The results demonstrate that any changes in the geometrical dimensions of the cantilever and in the fluid properties may influence the accuracy of the model. Furthermore, due to the considerable effect of tip-sample separation on the resonance, some models are restricted to be applicable only in the circumstances of free liquid.

1. Introduction

Dynamic responses of microcantilever beams have many applications, ranging from ultrasensitive mass measurements [1] to nanoscale imaging by atomic force microscopy. Atomic force microscopy, a member of the scanning probe microscopy family, is a vigorous tool for acquiring high resolution nanoscale surface images [2]. It generates real-space images by "feeling" the sample surface rather than "looking at" it. Both mechanical and morphological properties of sample surfaces are obtained by a sharp tip at the end of the cantilever [3]. There are many advantages to operating an atomic force microscopy with the cantilever and sample immersed in liquid. These advantages involve the elimination of capillary forces, the reduction of van der Waal's forces and the ability to study biologically and technologically significant processes at liquid–solid interfaces [4–6]. However, there have been certain disadvantages to imaging in contact mode in a liquid environment, where damage to biological samples would be the most common defect occurring in such experiments [7,8]. By using tapping mode AFM, such damages are greatly reduced. As the operation of AFM in viscous fluids (liquids or gases) considerably affects the microcantilever frequency response, some theoretical models have been described for vibration of the cantilever in a liquid environment. These studies demonstrate that liquid viscosity plays a key role in the frequency response of microcantilevers in AFM or microelectromechanical systems (MEMS), whereas for cantilevers of macro scale, the effects of viscosity could be negligible [9]. In a new type of noncontact AFM identified as the magnetic AC mode (MAC), which was introduced by Han et al., the signal-to-noise ratio (SNR) was improved. With a higher signal-to-noise ratio, cantilevers with lower force-constant and smaller motion amplitude can be used and so, probable damage

* Corresponding author.
E-mail address: hkorayem@iust.ac.ir (M.H. Korayem).

doi:10.1016/j.scient.2011.08.009

to the sample is reduced, probe stiffness is maintained and consequently higher resolution in liquid environment imaging can be gained [10]. In principle, using the MAC mode develops the utility of AFM for the imaging of a wider range of living samples, such as weak cells or even multilayer tissues [11].

The motion of the cantilever in air near a surface with an intermediate substrate contact has been described with simple and well-known models, such as those in [12–16]. For considering higher mode effects [17] or effects of a liquid environment [18], a continuous model describing the full shape of the cantilever is required. Having extended this model, the hydrodynamic forces on the magnetically oscillated cantilever could be determined for a range of tip-sample separations. One pertinent issue concerning a vibrating cantilever above a surface, when the whole system is dipped into a liquid, is squeezed film damping, which is an effect of the liquid or gas squeezing into the structures. In each oscillation, the fluid is squeezed onto the surface and thus an extra drag force (damping) is generated. Such an event has substantial influence on resonance frequency, the quality factor and the vibration amplitude of the cantilever. Accelerometers, pressure sensors and actuators usually take advantage of these effects for optimization of their designs [19].

In this paper, approximate models for calculating the resonance frequency of a microcantilever immersed in a viscous liquid are reviewed and by regarding preliminary assumptions and approximations, the accuracy and advantages of the models are discussed. There are certain deficiencies associated with some modeling methods due to the applied simplifications. These deficiencies may include the hypothesis of an inviscid fluid or the incapability of calculating the squeezed film damping effect near a solid surface.

2. Theoretical modeling

In general, the motion of the cantilever in liquid causes a fraction of the liquid mass to move along with the cantilever and therefore the effective vibrational mass is increased due to the coupled mass of liquid with the mass of the cantilever. Also, an extra damping force would be exerted on the system due to the viscous friction property of the liquid. In tapping mode AFM, the cantilever moves close to a surface that gives rise to an additional damping effect related to the squeezed liquid.

2.1. Resonance frequency in free liquid

There are generally two types of modeling to obtain the resonance frequency of a cantilever in liquid. Methods which observe squeezed film damping are more suitable for estimating resonances than those which neglect the effect of a solid wall on the dynamic response of a cantilever. In this section, three approximate methods for modeling cantilever motion far from the surface are examined. The inviscid model assumes that the liquid has a negligible viscosity and the cantilever has a uniform cross section with its width much smaller than its length. The viscous model considers damping, as well as the additional mass effect of the liquid, and determines the approximate resonances by an iterative process with an estimated initial value of resonance frequency in air. In the effective mass replacement model, the mere cantilever mass is replaced with the total vibrational effective mass (i.e. considering added fluid mass) in the equation of the resonance frequency in a vacuum environment.

2.1.1. Sader's inviscid model, vibration in a hypothetically inviscid fluid

The theoretical model consists of some general presumptions and approximations as follows [20]:

1. The cross section of the cantilever is uniform over its entire length.
2. The length of the cantilever exceeds its nominal width.
3. The cantilever is an isotropic linearly elastic solid and internal frictional effects are negligible.
4. The motion amplitude of the cantilever is much smaller than its other geometrical dimensions.

Furthermore, all torsional effects will be neglected and only the flexural mode of vibration will be considered. These approximations are usually satisfied in practical interests, as for microcantilevers used in atomic force microscopy. Due to the small motion amplitude, the nonlinear effects of convective inertia would be neglected and therefore hydrodynamic forces acting on the cantilever would be a linear function of its displacement. The velocity field at any point of the cantilever is approximated to that of a long rigid beam with identical oscillation amplitude. The resonance frequency of a multilayer cantilever with a uniform cross section in an inviscid liquid is given by [20]:

$$\frac{\omega_r}{\omega_{vac}} = \left(1 + \frac{\pi \rho_f b}{4 \sum \rho_i h_i}\right)^{-\frac{1}{2}}, \tag{1}$$

where ω_r is the resonance frequency in liquid, ω_{vac} is the resonance frequency in vacuum, ρ_i is the mass density of each layer of the composite cantilever, h_i is the thickness of each layer, b is the width of the cantilever and ρ_f is the density of the surrounding liquid.

2.1.2. Vancura's viscous model, vibration in viscous fluid, iterative process

In this modeling method, a general form of the resonance frequency of the cantilever in free liquid, according to its substantial viscosity, is given based on the solution of the fluidic vibrational equation of the cantilever. Due to Sader [20], for a liquid in which a cantilever is moving, the equation of motion is written as:

$$-\nabla.\hat{p} + \eta \nabla^2 \hat{u} = -i\rho_f \omega \hat{u}, \quad \nabla.\hat{u} = 0, \tag{2}$$

where $\hat{u}$ is the velocity field, $\hat{p}$ is the pressure, η is the dynamic viscosity of the fluid and ω is the angular frequency. In Eq. (2), all nonlinear effects of convectional inertia are neglected. The general form of the Fourier solution of the hydrodynamic force acting on the cantilever is written as:

$$\hat{F}_{\text{hydro}}(x \mid \omega) = \frac{\pi}{4} \rho_f \omega^2 b^2 \Gamma(\omega) \hat{W}(x \mid \omega), \tag{3}$$

in which the hydrodynamic function, $\Gamma(\omega)$, is dimensionless and acquired from Eq. (2). For a cylindrical cantilever, the exact solution of $\Gamma(\omega)$ is well known as:

$$\Gamma_{\text{circ}}(\omega) = 1 + \frac{4iK_1\left(-i\sqrt{i\,\text{Re}}\right)}{\sqrt{i\,\text{Re}}\,K_0\left(-i\sqrt{i\,\text{Re}}\right)}. \tag{4}$$

The Reynolds number, Re, is proportional to the squared diameter of the cylinder (the dominant scale). K_0 and K_1 are the modified Bessel function of type three. The hydrodynamic function for a rectangular beam is:

$$\Gamma_{\text{rect}}(\omega) = \Omega(\omega)\Gamma_{\text{circ}}(\omega), \tag{5}$$

where $\Omega(\omega)$ is the correction function for a beam with a rectangular cross-section. The hydrodynamic loading can be stated in two terms. The first term, denoted by g_1, is related to the damping force, which is due to the fact that the motion of the fluid is not necessarily in the same phase as that of the cantilever. This term is called the liquid damping coefficient, which is related to the velocity of the cantilever. The second term, denoted by g_2, is related to the acceleration of the cantilever and is the result of the oscillatory motion of the coupled liquid and cantilever masses. The general form of hydrodynamic loading is expressed by combining the two terms as [20,21]:

$$F_h = -g_1\dot{u} - g_2\ddot{u}. \tag{6}$$

$u = u(x, t)$ is the vertical displacement, g_1 is the liquid damping term and g_2 is the added fluid mass term in unit length of the cantilever. The following equations are used to calculate the terms g_1 and g_2:

$$g_1 = \pi\eta\,\mathrm{Re}\,\Gamma_i(\mathrm{Re}), \tag{7}$$

$$g_2 = \frac{\eta\,\mathrm{Re}}{2f_r}\Gamma_r(\mathrm{Re}), \tag{8}$$

where Γ_r and Γ_i are the real and imaginary parts of the hydrodynamic function of a rectangular beam, respectively, which is written as:

$$\Gamma(\mathrm{Re}) = \Omega(\mathrm{Re})\left[1 + \frac{4iK_1\left(-i\sqrt{i\,\mathrm{Re}}\right)}{\sqrt{i\,\mathrm{Re}}\,K_0\left(-i\sqrt{i\,\mathrm{Re}}\right)}\right], \tag{9}$$

in which Reynolds number, Re, is dependent upon the resonance frequency, f_r, of the cantilever in liquid:

$$\mathrm{Re} = \frac{\pi\rho_f b^2 f_r}{2\eta}. \tag{10}$$

We see that the Reynolds number depends on the oscillation frequency of the cantilever in liquid, while f_r is an unknown parameter, the value of which is of interest to us. The resonance frequency of a cantilever in free liquid is calculated based on the resonance frequency in vacuum:

$$f_r = f_0\frac{1}{\sqrt{1 + Lg_2/M}}\sqrt{1 - \frac{1}{2Q_{\mathrm{tot}}^2}}, \tag{11}$$

where L is the length of the cantilever and M is its mass. Q_{tot} is the quality factor of the cantilever immersed in liquid by considering all dissipations including both structural and liquid damping. It should be noted that the natural frequency is measured in the no-load condition, while the resonance frequency is connected to the effects of loadings. The resonance frequency is always smaller in value than the natural frequency. For a composite cantilever with different layers of length, L, the resonance frequency in vacuum is calculated by:

$$f_0 = \frac{1}{2\pi}\left(\frac{\lambda_0}{L}\right)^2\sqrt{\frac{\Sigma_i E_i I_i}{b\sum_i \rho_i h_i}}, \tag{12}$$

in which $\lambda_0 = 1.875104$ denotes the fundamental mode of vibration, I_i is the flexural moment of inertia and E_i is the modulus of elasticity of each layer. For a rectangular cross section, the moment of inertia of each layer with respect to the neutral axis is calculated by:

$$I_i = b\left(\frac{h_i^3}{12} + h_i(z_i - z_N)^2\right). \tag{13}$$

$z_i - z_N$ is the distance between the neutral axis and the center of the ith layer. The quality factor of a microstructure dipped in liquid (Q_{tot}) takes into account liquid damping as well as internal damping, and is expressed by:

$$\frac{1}{Q_{\mathrm{tot}}} = \frac{1}{Q_{int}} + \frac{1}{Q_{\mathrm{fluid}}}, \tag{14}$$

with Q_{int} being the intrinsic quality factor and Q_{fluid} the fluid contribution to the quality factor. For a resonant microcantilever in a liquid like water, in an out-of-plane mode (vertical vibration), the term Q_{fluid} is the dominant part of the total Q-factor. Therefore, we neglect the term Q_{int} and the total quality factor is approximated by:

$$Q_{\mathrm{tot}} \approx Q_{\mathrm{fluid}} = 2\pi f_0\frac{\sqrt{1 + Lg_2/M}}{Lg_1/M}. \tag{15}$$

From Eqs. (10) and (11), we find that a self-consistent calculation for defining the resonance frequency is necessary. This is done by first calculating the Reynolds number according to Eq. (10) with the resonance frequency in air as an initial value. The value of the obtained Reynolds number is then used to calculate the values of g_1 and g_2 according to Eqs. (7) and (8). These calculated values can be used to obtain the new resonance frequency in liquid according to Eq. (11), and the new Reynolds number according to Eq. (10).

This iterative process is continued until self-consistency is reached [22].

2.1.3. Effective mass replacement (EMR) model

According to recent investigations, the added fluid mass represents the main role in the changes of the resonance frequency of microcantilevers in free liquid [22]. Therefore, we have replaced the cantilever mass in the equation of resonance frequency in vacuum with the total effective mass including the part of the liquid mass that is forced into motion by the cantilever vibrations. According to Eq. (12), an approximate formula for estimating the resonance peaks is derived as:

$$f_r = \frac{1}{2\pi}\left(\frac{\lambda_0}{L}\right)^2\sqrt{\frac{\Sigma_i E_i I_i}{b\Sigma_i\rho_i h_i + \rho_a}}. \tag{16}$$

Due to Greenspon [23], the added fluid mass density, ρ_a, can be calculated by:

$$\rho_a = 0.6\rho_f L^{1/2}b^{3/2}. \tag{17}$$

By representing the beam as a string of beads, Hosaka et al. [24] gave another expression for ρ_a as:

$$\rho_a = \frac{1}{12}\pi\rho_f b^2 + \frac{3}{4}\pi b\sqrt{\frac{2\rho_f\eta}{\omega}}, \tag{18}$$

in which ω is the vibrating (circular) frequency of the cantilever.

2.2. Frequency response close to a surface

2.2.1. Rankl's method

In this part, by approximating the various forces acting on the cantilever, the equation of motion of the cantilever and the boundary conditions are given. By assuming harmonic motion with excitation frequency, ω, frequency responses of microcantilevers are simulated for a definite range of ω, and the resonance peaks are then indicated as resonance frequencies of the cantilevers for various tip-sample separations [25]. A

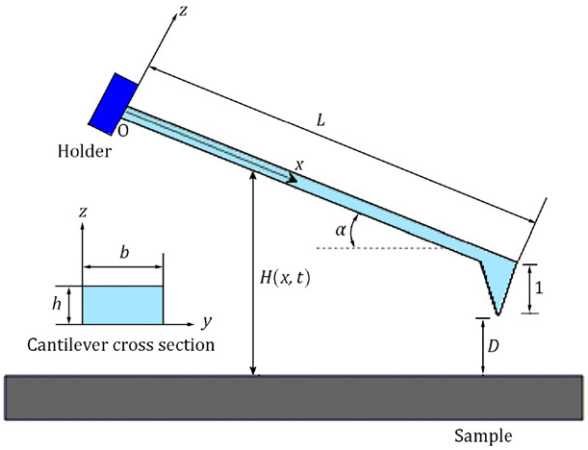

Figure 1: The model used for the theoretical analysis of the cantilever oscillation in liquid in the vicinity of the sample surface. A cantilever with homogeneous rectangular cross section and a sharp tip at the end of the cantilever is shown.

schematic view of an AFM cantilever vibrating in liquid near a surface is shown in Figure 1.

As shown in Figure 1, the cantilever is slightly inclined at angle α, and has length L, width b, thickness h, cross section area A, tip height l and equilibrium tip-sample separation D. $H(x, t)$ is the distance between any point of the cantilever and the sample surface at any time of the vibration. The cantilever is immersed in a liquid with density, ρ_f, and dynamic viscosity, η. Due to the Euler–Bernoulli equation for a beam oscillating in small amplitudes, the equation of motion is written as:

$$EI\frac{\partial^4 u}{\partial x^4} + \mu^*\frac{\partial^2 u}{\partial t^2} = F(x, t), \tag{19}$$

where μ^* (kg/m) is the linear mass density of the cantilever in liquid, and $F(x, t)$ (N/m) is the total force acting on the unit length of the cantilever. In this case, the total force consists of magnetic driving force, F_m, joint mass density, F_t, at the end of the cantilever, and hydrodynamic force, F_h, written as:

$$F = F_m + F_t + F_h, \tag{20}$$

$$F_m = S\,\mathrm{e}^{-i\omega t}, \tag{21}$$

$$F_t = m_t^*\frac{\partial^2 u}{\partial t^2}\delta(x - L), \tag{22}$$

$$F_h = F_s + F_v, \tag{23}$$

where S is the strength of the magnetic force, m_t^* is the joint mass density (the mass of the tip of the AFM cantilever) and $\delta(x - L)$ is the Dirac's delta function. The hydrodynamic force, F_h, consists of two parts as follows:

1. The force associated with the viscous friction of the liquid is expressed as:

$$F_v = -\gamma_\infty\frac{\partial u}{\partial t}. \tag{24}$$

For a harmonically oscillating sphere, the closed form solution of the friction coefficient, γ_s, was derived in [26]:

$$\gamma_s = 3\pi\eta d + \frac{3}{4}\pi d^2\sqrt{2\rho_f\eta\omega}, \tag{25}$$

with d being the diameter of the sphere. A rectangular cantilever can be considered as a string of closely arranged spheres with the diameter equal to width b of the cantilever. Then, the friction coefficient, γ_∞, of the cantilever is the sum of the friction coefficients of the spheres. For AFM cantilevers, the resonance frequency is in the order of 100 kHz and both the penetration depth and cantilever width are in the same order of 10 micrometers, so using this spherical model is possible. The penetration depth is $\delta = \sqrt{\frac{2\eta}{\omega\rho}}$ (η and ρ are, respectively, liquid dynamic viscosity and density and ω is resonance frequency) [26].

Since the number of spheres per unit length of the microcantilever is $1/b$ (b the cantilever width), γ_∞ is given by [24,26]:

$$\gamma_\infty \approx 3\pi\eta + \frac{3}{4}\pi b\sqrt{2\rho_f\eta\omega_r}. \tag{26}$$

In Eq. (26), the resonance frequency of the cantilever in free liquid, ω_r, is obtained through the second method (viscous model) discussed previously.

2. The effect of the surface at small cantilever-sample separations gives rise to an additional force. Considering the liquid bounded between the surface and the cantilever, when the cantilever approaches the surface, the liquid is consequently squeezed and has a tendency to move out of confinement. Thus, the viscous resistance generates an extra force, which is dependent on the distance between the cantilever and the sample surface. The so-called squeezed film damping force has a substantial effect on the motion of the cantilever and is written as:

$$F_s = -\eta b^3\frac{1}{H^3}\frac{\partial u}{\partial t}. \tag{27}$$

In typical AFM experiments, the cantilever is usually inclined at an angle of $\alpha = 15°$, with respect to the horizontal surface. As a result, distance h is dependent on coordinate x and consequently the distribution of force F_s along the cantilever is not uniform. For large distances, force density, F_s, is nearly constant along the cantilever (denoted by F_s^e) and for small distances, most force is concentrated at the end of the cantilever (denoted by F_s^c), which is equal to the integral of the F_s along the cantilever. In order to combine the two approximations into a single model, a weight function, $w(D)$, is used:

$$F_s = F_s^c(1 - w(D)) + F_s^e w(D), \tag{28}$$

for which the weight function should be zero for small tip-sample separations and one for large separations [25]. According to Figure 1, the distance between the cantilever and the sample surface at any time and location is:

$$H(x, t) = D + l + (L - x)\sin\alpha + u(x, t). \tag{29}$$

It is clear from Eq. (29) that distance $H(x, t)$ and, thereby, the squeezed film damping are functions of time. However, under most operating conditions of the tapping mode, vertical displacement $u(x, t)$ is in the range of several dozen to several hundred nanometers, which is 2–3 orders of amplitude smaller than the constant part of the $H(x, t)$. By neglecting the time-dependent part of the cantilever-sample distance, we have:

$$H_0 = H(0) = D + l + L\sin\alpha, \tag{30}$$

$$H_L = H(L) = D + l, \tag{31}$$

and the forces F_s^e and F_s^c as:

$$F_s^e = -\gamma_0\frac{1}{H_L^3}\frac{\partial u(x, t)}{\partial t}, \tag{32}$$

$$\begin{aligned} F_s^c &= -\eta b^3\delta(x - L)\frac{\partial u}{\partial t}\int\frac{1}{H(x)^3}\,\mathrm{d}x \\ &= -V_0\frac{L}{2}\frac{H_L + H_0}{H_L^2H_0^2}\delta(x - L)\frac{\partial u(L, t)}{\partial t}, \end{aligned} \tag{33}$$

where γ_0 and V_0 are the constant force strength and point force strength, respectively. Finally, the equation of motion of the cantilever and its boundary conditions are as:

$$EI\frac{\partial^4 u}{\partial x^4}+\mu^*\frac{\partial^2 u}{\partial t^2}=S\,e^{-i\omega t}-\left(\gamma_\infty+\gamma_0\frac{1}{H_L^3}w(D)\right)\frac{\partial u}{\partial t},$$

$$u(0,t)=0,\qquad u'(0,t)=0,\qquad u''(L,t)=0,$$

$$u'''(L,t)=-\frac{1}{EI}\left(m_t^*\frac{\partial^2 u}{\partial t^2}-V_0\frac{L}{2}\frac{H_L+H_0}{H_L^2H_0^2}\frac{\partial u(L,t)}{\partial r}(1-w(D))\right). \quad (34)$$

The harmonical analytical solution of Eq. (34) is:

$$u(x,t)=\left(A\,e^{\beta x}+B\,e^{-\beta x}+C\,e^{i\beta x}+D\,e^{-i\beta x}\right)e^{-i\omega t}, \quad (35)$$

in which A, B, C, D and term β are determined through the solution of Eq. (34) (see the Appendix of [25]).

2.2.2. Modal analysis

The modal analysis was used by Korayem and Ebrahimi in the dynamic analysis of tapping-mode AFM cantilevers [27]. In this model, the hydrodynamic forces are also applied by added mass and added damping. The bending behavior of an AFM cantilever in liquid can be written, using beam vibrating formulation, by the following partial differential equation:

$$EI\frac{\partial^4 u}{\partial x^4}+\rho A\frac{\partial^2 u}{\partial t^2}+c\frac{\partial u}{\partial t}=F(x,t), \quad (36)$$

where c represents the damping coefficient. $F(x,t)$ is the force applied on the cantilever per unit length of the cantilever at any time. It is composed of forces due to tip-sample interaction (F_{ts}), hydrodynamic forces due to liquid around the cantilever (F_{liq}), and excitation force (F_{exc}) applied on the cantilever:

$$F(x,t)=F_{\text{exc}}(x,t)+F_{\text{liq}}(x,t)+F_{ts}(x,t). \quad (37)$$

Researchers have approximated hydrodynamic forces to be in proportion with the cantilever vibration acceleration and velocity as [25]:

$$F_{\text{liq}}(x,t)=-\rho_a\frac{\partial^2 u}{\partial t^2}-c_a\frac{\partial u}{\partial t}, \quad (38)$$

where ρ_a is the additional mass, which is gained, based on Eq. (17) or (18). The additional damping coefficient, due to hydrodynamic effects (c_a), consists of two parts:

$$c_a=\gamma_\infty+\gamma_s. \quad (39)$$

The coefficient γ_∞ is the hydrodynamic damping when the cantilever is vibrating in free liquid (far from the sample surface), which is gained based on Eq. (26), and the damping coefficient of the squeezed film damping is gained by:

$$\gamma_s=\frac{\eta b^3}{H(x,t)^3}, \quad (40)$$

where $H(x,t)$ is the transient distance between the cantilever and surface, and is gained by Eq. (29). Obviously, γ_∞ is a constant, but γ_s depends on location and time. The separation of the cantilever tip from the sample is:

$$d_{ts}=D+u(L,t). \quad (41)$$

Using Eqs. (36)–(38), the governing equations can be written as:

$$EI\frac{\partial^4 u}{\partial x^4}+(\rho A+\rho_a)\frac{\partial^2 u}{\partial t^2}+(c+c_a)\frac{\partial u}{\partial t}=F_{ts}(x,t)+F_{\text{exc}}(x,t). \quad (42)$$

Table 1: Properties of the layers of composite cantilevers and the surrounding liquid.

Material	ρ, ρ_f (kg/m^3)	E (GPa)	η(kg/m s)
Single-crystal silicon	2330	170	–
Silicon oxide	2200	85.8	–
Silicon nitride	3100	290	–
Water	998.2	–	8.94×10^{-4}

F_{ts} is the tip-sample interaction, which is applied on the cantilever tip:

$$F_{ts}=\begin{cases}F_{vdw}(d_{ts})\cos\alpha & d_{ts}>a_0\\ (F_{vdw}(a_0)+F_{\text{DMT}})\cos\alpha & d_{ts}\le a_0.\end{cases} \quad (43)$$

In Eq. (43), $F_{vdw}(d_{ts})=-HR/(6d_{ts}^2)$ is the van der Waals force and $F_{\text{DMT}}=\frac{4}{3}E^*\sqrt{R}(a_0-d_{ts})^{3/2}$ is the repulsive contact force. H is the Hamakar constant, a_0 is the intermolecular distance, R is the tip cone radius, and E^* is the effective elastic modulus given by:

$$E^*=[(1-\upsilon_t^2)/E_t+(1-\upsilon_s^2)/E_s]^{-1},$$

in which E_t, E_s, υ_t and υ_s are the elastic module and Poisson ratios of the tip and sample, respectively. F_{exc} is the magnetic harmonic excitation force. By setting $c_{\text{tot}}=c+c_a$ and $\rho_{\text{tot}}=\rho A+\rho_a$, and using delta functions, Eq. (42) can be written as:

$$EI\frac{\partial^4 u}{\partial x^4}+\rho_{\text{tot}}\frac{\partial^2 u}{\partial t^2}+c_{\text{tot}}\frac{\partial u}{\partial t}=F_{ts}(x,t)\delta(x-L_1)+F_{\text{exc}}(x,t), \quad (44)$$

where L_1 is the position of the tip from the beginning of the cantilever, and $\delta(x-L_i)$ is the delta function. The boundary conditions are as the boundary conditions of a clamped-free cantilever. The equation can be solved using modal analysis for a continuous beam model [27].

3. Simulation results and discussion

According to the five modeling methods discussed in previous parts, the resonance frequency of microcantilevers with variable widths in liquid far from the sample surface will be compared. It should be noted that Vancura's viscous model [22] (Section 2.1.2), Rankl's method (Section 2.2.1) and Modal analysis (Section 2.2.2) consider both effective damping and added fluid mass in calculating the resonance frequency, while the first approximate method, i.e. Sader's inviscid modeling (Section 2.1.1) and effective mass replacement model (Section 2.1.3) neglect the effect of viscous friction damping on the resonance frequency. However, their results are almost close to the experimental results, since the effect of viscous damping in reducing the resonance frequency in free liquid is much smaller in comparison to the effect of added fluid mass. Table 1 shows the mechanical properties of water and composite cantilevers, which consist of a single crystal silicon layer (5 μm) in the center and two layers of oxide silicon (2.2 μm) and nitride silicon (1 μm) on top.

Table 2 shows the resonance frequency values acquired from various methods for cantilever geometries of 200 μm length, 8.2 μm thickness and four different widths, featuring 50, 100, 140 and 186 μm immersed in free water.

The results show that when we use a wider cantilever, the resonance frequency shifts towards lower values, due to an increase in the effective vibrating mass. This is because the

Table 2: Comparison of various methods in calculating the resonance frequencies of four microcantilevers vibrating in water far away the surface with the experimental data. The cantilevers have a 200 μm length, 8.2 μm thickness and variable widths (frequencies given in kHz).

Cantilever width (μm)	f_{Rankl}	$f_{Viscous}$	$f_{Inviscid}$	f_{EMR}	f_{Modal}	$f_{Meas.}$ [22]
50	145.1	161	168.7	145.1	145.1	165.9
100	126.7	126.3	130.6	126.6	126.7	142.2
140	118.2	110.5	113.7	118.1	118.2	129.7
186	111.3	98.2	100.5	111.2	111.3	120.5

Table 3: The ratio of the theoretical to measured resonance frequencies of four microcantilevers vibrating in water far away the surface (details as in Table 2).

Cantilever width (μm)	$f_{Rankl}/f_{Meas.}$	$f_{Viscous}/f_{Meas.}$	$f_{Inviscid}/f_{Meas.}$	$f_{EMR}/f_{Meas.}$	$f_{Modal}/f_{Meas.}$
50	0.87	0.97	1.02	0.87	0.87
100	0.89	0.89	0.92	0.89	0.89
140	0.91	0.85	0.88	0.91	0.91
186	0.92	0.81	0.83	0.92	0.92

cantilever mass is proportional to its width, and also the mass of liquid forced into motion by the oscillation of the cantilever is changed with the width dimension.

The ratio of theoretical predictions to experimental resonance frequencies are shown in Table 3. According to Table 3, for comparatively thick cantilevers of Table 2, the accuracies of resonance frequencies determined from Rankl's method as well as the Effective Mass Replacement (EMR) method are clearly enhanced, whereas it is seen that viscous modeling and the inviscid method gradually lose their preciseness by increasing the width of the cantilever. The modal results are similar to those of the Rankl method and it seems that the theoretical frequency to measured data ratio remains almost constant. The discrepancy between Rankl and EMR methods in large tip-sample separations is so small that we can consider their values as identical. Their similarity is probably due to the fact that water has a low viscosity, so the viscous friction damping has very little effect on such thick cantilevers. If a liquid with higher viscous resistance was used instead, the Rankl and EMR methods would show more pronounced different resonance frequencies. The trend of changes in resonance frequencies in the Rankl (or EMR) method indicates that by choosing a cantilever with lower aspect ratio (the size of thickness divided by the size of width), the fluctuations of the results of these methods are less than those obtained by viscous or inviscid methods. Therefore, they show a better stability or less sensitivity when the width dimension is changed. However, as shown in Table 2, for thick microcantilevers with a rather high aspect ratio (constant length and smaller width), the resonance frequencies of viscous or inviscid methods give better agreement with experimental values. For the following comparisons, we consider the Rankl and EMR as almost similar methods and then analyze their differences with other modeling methods.

Figure 2 shows the resonance frequency of cantilevers with 8.2 μm thickness and different widths. The slopes of the curves attributed to each method indicate that the resonance frequencies gained by viscous and inviscid models bear large changes by changing the widths of the cantilevers, but Rankl and EMR methods have smaller changes. Around the width of 100 μm, the results of all methods seem to be equal, and for widths larger than 100 μm, the resonance frequencies obtained from Rankl's method are predicted to show better agreement with real values.

Since the added liquid mass and the viscous damping are major effective factors, the differences in the results are mainly due to the differences in the calculation of those factors between the methods. Figure 3 shows the damping

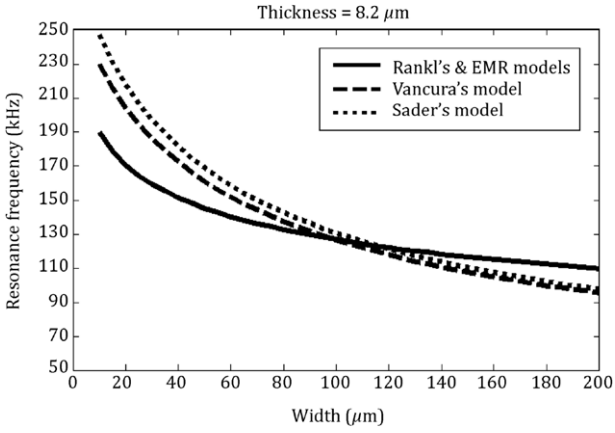

Figure 2: Diagram of the resonance frequency versus cantilever width for cantilevers with 200 μm length and 8.2 μm thickness for different modeling methods.

coefficient (a) and the added mass density (b) for different widths of the cantilever. Due to Figure 3(b), the closeness of added mass density values around the width of 100 μm may be the reason for the similarity of resonance frequencies obtained from different methods for thick cantilevers on which viscous damping has a minimal effect when separation between the cantilever and the sample surface is large. We then have compared the methods in calculating the resonance frequency of a thin cantilever with 200 μm length, 20 μm width, 0.6 μm thickness and 3 μm tip height. Frequency response curves (tuning curves) of the magnetically oscillated cantilever with a rectangular cross section immersed in a buffer solution, demonstrate a high dependency upon tip-sample separation. The buffer solution consists of 150 mM Nacl and 5 mM NaH_2PO_4. Tuning curves were recorded by varying the excitation frequency from 0.1 to 10 kHz in steps of 0.1 kHz, and by measuring the corresponding amplitudes of the cantilever response. The acquired amplitude–frequency curves from simulation show a good agreement with the experimental results of [25]. Resonance frequency determined from the peak of the tuning curve at the separation of 44 μm (a big separation) can be compared with the values of other modeling methods as shown in Table 4.

According to Table 4, the good agreement of Rankl or Vancura viscous data with those experimentally obtained, in comparison with other models, indicates that the viscous friction of the liquid greatly affects such a thin cantilever

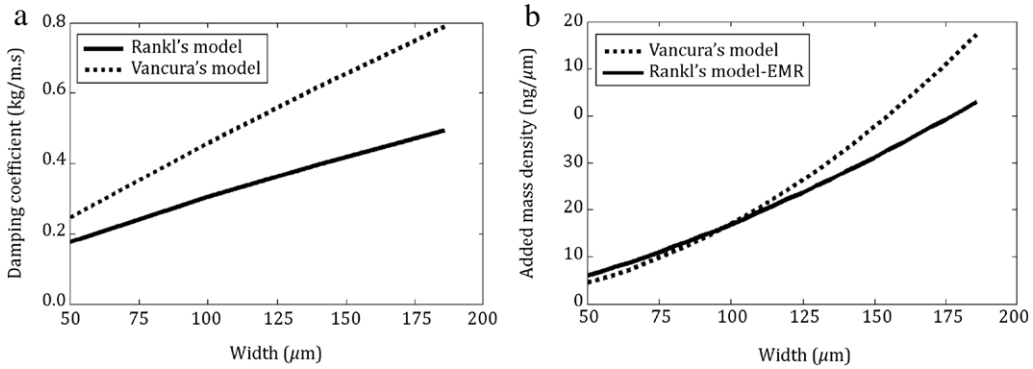

Figure 3: Comparison of the methods in calculating viscous damping coefficient and added fluid mass density for cantilevers of 200 μm length, 8.2 thickness and variable widths vibrating in water. (a) Damping coefficient changes for different widths. (b) Added fluid mass density changes for different widths.

Table 4: Theoretical resonance frequency of a thin cantilever vibrating in water at a large tip-sample separation (44 μm). The cantilever has 200 μm length, 0.6 μm thickness and 20 μm width.

Modeling method	Resonance frequency (kHz)	% Error
Rankl	3.150	0.96%
Viscous	3.153	1%
Inviscid	5.276	69%
EMR	3.849	23%
Experiment [25]	3.120	–

Table 5: Viscosities and densities of four fluids at $T = 27$ °C.

Fluid	Viscosity η (kg/m s)	Density ρ_f (kg/m^3)
Acetone	3.08×10^{-4}	785
CCl_4	8.79×10^{-4}	1590
Water	8.94×10^{-4}	997
1-butanol	2.47×10^{-3}	805

whose thickness is much smaller than its width and whose cross section area is comparatively small whereas the effect of viscosity is not considered using EMR and inviscid methods. From Figure 3, we also know that the added mass terms with this width are close to each other in these two methods. Changes of resonance frequency due to different thicknesses are shown in Figure 4. In this case, the Rankl and EMR methods gave similar results. As shown in Figure 4, for a cantilever of width 50 μm, the Rankl method gives lower values in comparison to other methods and by a gradual increase in width, the resonance frequencies of the Rankl method shift towards higher values while the predicted data of viscous and inviscid methods become closer. Also, the results are very close in cases where the cantilever width is 100 μm and in other cantilever widths the difference is higher.

Characteristics of four liquids are shown in Table 5. Tables 6 and 7 show the resonance frequencies of liquid-immersed microcantilevers with two different lengths in different liquids of Table 5 for comparing methods. The cantilevers have the mass density of 2320 kg/m^3 and the Young's modulus of 172.6 GPa. According to Tables 6 and 7, since the geometrical dimensions of the cantilevers are changed, the methods show different accuracy with respect to the measured resonance frequencies. In these two cases, the viscous model has the best agreement with the experimentally obtained values, while other models indicate fluctuations in their results for fluids of different properties.

EMR, Vancura and Sader models do not have the effect of the squeezed film damping in their models and, so, are not comparable with models that consider the effect of squeezed film damping, like the Rankl model. By using the modal method, the frequency response of rather thick silicon microcantilevers is simulated for various tip-sample separations in Figure 5, and so the effect of squeezed film damping can be observed. According to Figure 5, the four microcantilevers with different widths have disparate responses in the vicinity of a solid surface. As shown in Figure 5, when the cantilever approaches the sample, the maximum point of the tuning curves is shifted to lower quantities and the sharpness of the peaks is gradually smoothed. At larger cantilever widths, the reduction of the resonance frequency with a reduction in separation is greater.

If we notice the equation of squeezed film damping (Eq. (16)), it is obvious that this force is directly proportional to cubic width and inversely to cubic cantilever-sample distance. Thereby, the effect of this damping on the motion of the cantilever is higher if we drive a rather wide cantilever in the close vicinity of a surface.

Spring constants of the examined cantilevers would be a key factor in vibration analysis, which depends greatly on flexural stiffness, in which the thickness of the cantilever is an important parameter. The large thickness, which was held constant in the tuning curve simulations, shows its influence in the form of increasing resonance frequency and difficulty in excitation of the cantilever as well. Spring constant also depends on the width of the cantilever. In Figure 5, spring constants of the four cantilevers, with widths of 50, 100, 140 and 186 μm, are increased as 160.5 N/m, 321 N/m, 449.4 N/m and 597.1 N/m, respectively, but the resonances occur at lower values. In fact, the reduction in frequencies is due to the effect of added mass and squeezed film, which dominates the effect of the spring constant.

Figure 6 shows the diagrams of the resonance frequency versus cantilever width for two cantilevers (200 μm length and two thicknesses of (a) 8.2 μm thickness and (b) 2 μm thickness) in two closer separations of cantilever from the sample (25 m & 1 μm). It is seen that the slope of reduction in resonance frequency, by increasing cantilever width, is larger in closer separations.

For Rankl or Modal methods, which consider the added mass method, for a one layer cantilever we can write the resonance frequency far from the surface in a low viscosity liquid as:

$$\frac{1}{f_r^2} = \frac{kL^4\left(\rho + 0.6 \times \rho_f\sqrt{Lb/h^2}\right)}{Eh^2}, \tag{45}$$

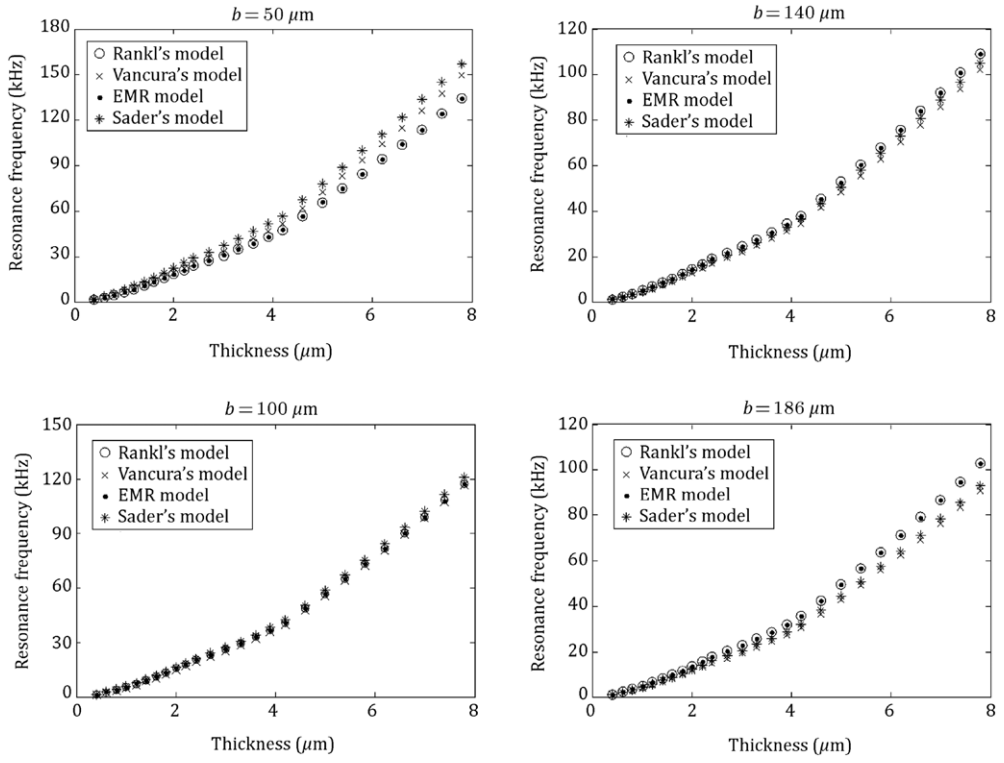

Figure 4: Diagrams of resonance frequency versus thickness for cantilevers with the same length and four different widths, based on various modeling methods.

Table 6: Resonance frequencies of a liquid-immersed cantilever with 197 μm length, 29 μm width and 2 μm thickness based on various methods (frequencies given in kHz, measured data from [28]).

Fluid	f_{Rankl}	$f_{Viscous}$	f_{EMR}	$f_{Inviscid}$	$f_{Meas.}$	$f_{Rankl}/f_{Meas.}$	$f_{Viscous}/f_{Meas.}$	$f_{EMR}/f_{Meas.}$	$f_{Inviscid}/f_{Meas.}$
Acetone	24.1	28.7	24.4	32.6	29.5	0.82	0.97	0.83	1.10
CCl_4	17.5	20.1	17.6	24.2	20.8	0.84	0.97	0.85	1.16
Water	21.6	24.3	21.9	29.6	25.2	0.86	0.96	0.87	1.17
1-butanol	23.5	23.4	24.1	32.3	24.1	0.98	0.97	1	1.3

Table 7: Resonance frequencies of a liquid-immersed cantilever with 397 μm length, 29 μm width and 2 μm thickness based on various methods (frequencies given in kHz, measured data from [28]).

Fluid	f_{Rankl}	$f_{Viscous}$	f_{EMR}	$f_{Inviscid}$	$f_{Meas.}$	$f_{Rankl}/f_{Meas.}$	$f_{Viscous}/f_{Meas.}$	$f_{EMR}/f_{Meas.}$	$f_{Inviscid}/f_{Meas.}$
Acetone	4.9	6.3	5.1	8.0	6.35	0.77	0.99	0.80	1.26
CCl_4	3.5	4.2	3.7	5.9	4.22	0.83	0.99	0.88	1.40
Water	4.4	5.0	4.6	7.3	5.04	0.87	0.99	0.91	1.45
1-butanol	4.4	4.2	5.1	7.9	3.93	1.12	1.07	1.30	2.01

where k is a constant and f_r is the resonance frequency. From this formula, we can see that the density of the liquid has an inverse relation with the square of the resonance frequency.

For a one layer silicon cantilever, with density of 2330 kg/m^3 and Young's modulus of 170 GPa, the log–log plot of the resonance frequency versus cantilever thickness (h), cantilever width (b) and cantilever length (L) gives the following formulas for far separations from the sample, and the low viscosity of the liquid. The base dimensions are $h = 10$ μm, $W = 50$ μm and $L = 200$ μm.

$$\frac{1}{f^2} = 2.3 \times 10^{-25} h^{-2.88}, \tag{46}$$

$$\frac{1}{f^2} = 5.33 \times 10^{-10} b^{0.2913}, \tag{47}$$

$$\frac{1}{f^2} = 2.2486 \times 10^{5} L^{4.2913}. \tag{48}$$

4. Conclusions

Simulation results of the approximate resonance frequency of microcantilevers vibrating in free liquid were compared to experimental data, and the accuracy of various methods was studied. By presenting a typical modeling of an AFM cantilever in practical experiments and then an analytical solution of the equation of motion of the cantilever by approximating the hydrodynamic forces acting on it, the frequency response of several microcantilevers were simulated at various tip-sample separations. Microcantilevers with different dimensions have different resonance frequencies in a liquid environment.

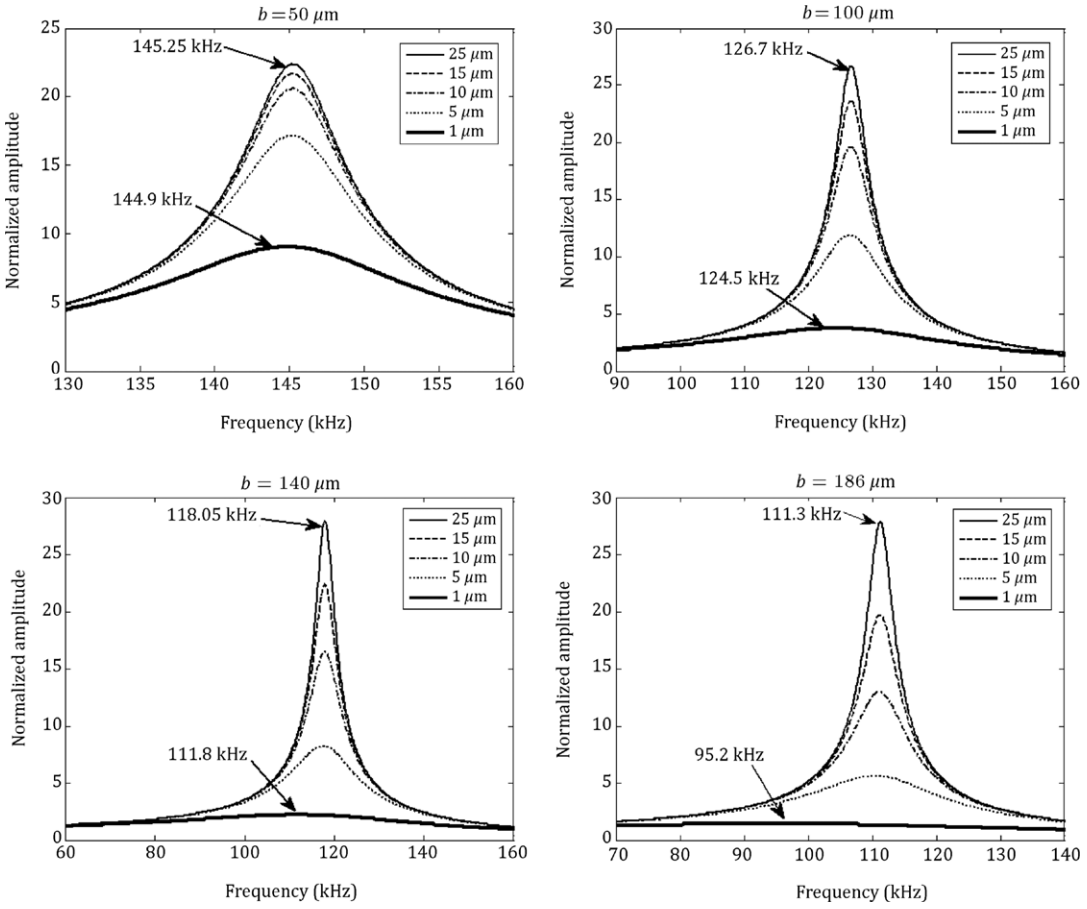

Figure 5: Simulations of frequency responses of four water-immersed microcantilevers with 200 μm length, 8.2 μm thickness and different widths featuring 50, 100, 140 and 186 μm are shown for various tip-sample separations. The effect of hydrodynamic forces particularly the squeezed film damping is such that the resonance peaks occur at lower values for large widths.

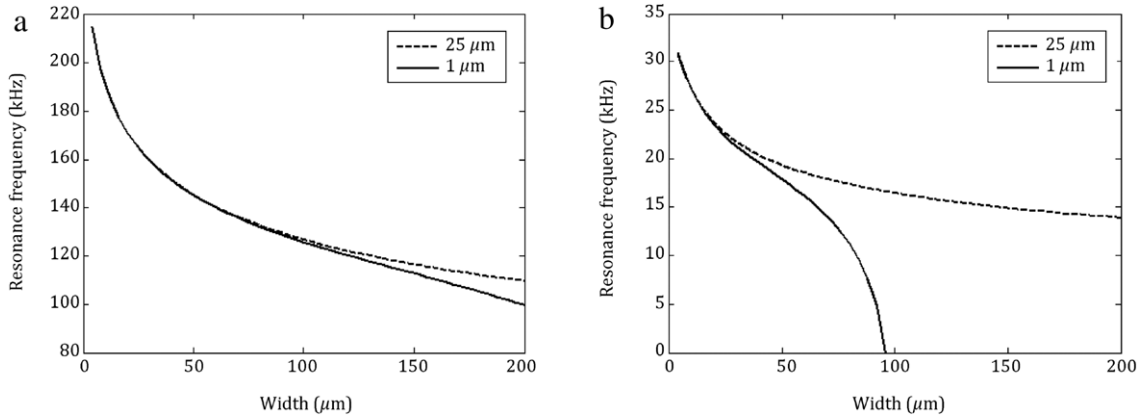

Figure 6: Diagram of the resonance frequency versus cantilever width for a cantilever with 200 μm length and (a) 8.2 μm thickness (b) 2 μm thickness in two different separations (25 & 1 μm) from the sample.

Based on the frequency changes, due to the variable widths and different fluids, the sensitivity of various methods with respect to geometrical parameters as well as liquid properties was observed. In large tip-sample separations, the modeling methods of Rankl and Vancura (viscous model) displayed more agreeable results for a thin cantilever with a small cross section area, because of consideration of the effect of viscous friction damping on the oscillatory motion of the cantilever. For slightly thicker cantilevers vibrating in different liquids, the viscous model has the best agreement with experimentally obtained values. For much thicker cantilevers, the methods of Rankl and effective mass replacement show higher accuracy and stability by changing the dimensions of the width, however, fluctuations in their results occurred as the liquid properties were changed. As the cantilever got closer to the solid surface with constant velocity, the hydrodynamic loading had its effect on shifting the

resonance peaks of the amplitude–frequency curves towards lower values and smaller motion amplitudes. This effect was observed using the Rankl modeling method through which the effect of squeezed liquid can be considered in the damping term. However, some other methods are applicable only for big tip-sample separations where we can neglect the effect of the sample surface on the resonance frequency.

References

[1] Berger, R., Gerber, Ch., Land, H.P. and Gimzewski, J.K. "Micromechanics: a toolbox for femtoscale science: towards a laboratory on a tip", *Microelectron. Eng.*, 35, p. 373 (1997).

[2] Binnig, G., Quate, C.F. and Gerber, Ch. "Atomic force microscope", *Phys. Rev. Lett.*, 56, p. 930 (1986).

[3] Morris, V.J., Kirby, A.R. and Gunning, A.P., *Atomic Force Microscopy for Biologists*, Imperial College Press, London (1999).

[4] Rugar, D. and Hansma, P.K. "Atomic force microscopy", *Phys. Today*, 43, p. 23 (1990).

[5] Drake, B., Prater, C.B., Weisenhorn, A.L., Gould, S.A., Albrecht, T.R., Quate, C.F., Cannell, D.S., Hansma, H.G. and Hansma, P.K. "Imaging crystals, polymers, and processes in water with the atomic force microscope", *Science*, 243, p. 1586 (1989).

[6] Weisenhorn, A.L., Hansma, P.K., Aibrecht, T.R. and Quate, C.F. "Forces in atomic force microscopy in air and water", *Appl. Phys. Lett.*, 54, p. 2651 (1989).

[7] Saenz, J.J., Garcia, N., Grutter, P., Meyer, E., Heinzelmann, H., Wresendanger, R., Rosenthaler, L., Hidber, H.R. and Guntherodt, H.I. "Observation of magnetic forces by the atomic force microscope", *J. Appl. Phys.*, 62, p. 4293 (1987).

[8] Martin, Y. and Wickramasinghe, H.K. "Magnetic imaging by force microscopy with 1000 a resolution", *Appl. Phys. Lett.*, 50, p. 1455 (1987).

[9] Van Eysden, C.A. and Sader, J.E. "Frequency response of cantilever beams immersed in viscous fluids with applications to the atomic force microscope: Arbitrary mode order", *J. Appl. Phys.*, 101(4), p. 044908 (2007).

[10] Han, W., Lindsay, S.M. and Jing, T. "A magnetically driven oscillating probe microscope for operation in liquids", *Appl. Phys. Lett.*, 69, p. 4111 (1996).

[11] Ge, G., Han, D., Lin, D., Chu, W., Sun, Y., Jiang, L., Ma, W. and Wang, C. "MAC mode atomic force microscopy studies of living samples, ranging from cells to fresh tissue", *Ultramicroscopy*, 107, p. 299 (2007).

[12] Garcia, R. and San Paulo, A. "Attractive and repulsive tip-sample interaction regimes in tapping-mode atomic force microscopy", *Phys. Rev. B*, 60, p. 4961 (1999).

[13] Nony, L., Boisgard, R. and Aimé, J.P. "Nonlinear dynamical properties of an oscillating tip-cantilever system in the tapping mode", *J. Chem. Phys.*, 111, p. 1615 (1999).

[14] Marth, M., Maier, D., Honerkamp, J., Brandsch, R. and Bar, G. "A unifying view on some experimental effects in tapping-mode atomic force microscopy", *J. Appl. Phys.*, 85, p. 7030 (1999).

[15] Gotsmann, B., Seidel, C., Anczykowski, B. and Fuchs, H. "Conservative and dissipative tip-sample interaction forces probed with dynamic AFM", *Phys. Rev. B*, 60, p. 11051 (1999).

[16] Van de Water, W. and Molenaar, J. "Dynamics of vibrating atomic force microscopy", *Nanotechnology*, 11, p. 192 (2000).

[17] Stark, R.W. and Heckl, W.M. "Fourier transformed atomic force microscopy: tapping mode atomic force microscopy beyond the Hookian approximation", *Surf. Sci.*, 457, p. 219 (2000).

[18] Bao, M.H., *Handbook of Sensors and Actuators*, 1st ed. Elsevier (2000).

[19] Chu, W.H. "Tech. Rep. No. 2, DTMB, Contract NObs-86396(X)", Southwest Research Institute, San Antonio, Texas (1963).

[20] Sader, J.E. "Frequency response of cantilever beams immersed in viscous fluids with applications to the atomic force microscope", *J. Appl. Phys.*, 87, p. 64 (1998).

[21] Dufour, I., Heinrich, S.M. and Josse, F. "Strong-axis bending mode vibrations for resonant microcantilever (bio) chemical sensors in gas or liquid phase", *Proceedings of the 2004 IEEE International*, Montreal, August 23–27 (2004).

[22] Vancura, C., Dufour, I., Heinrich, S.M., Josse, F. and Hierlemann, A. "Analysis of resonating microcantilevers operating in a viscous liquid environment", *Sensors and Actuators A*, 141, p. 43 (2008).

[23] Greenspon, J.E. "Vibration of cross-stiffened and sandwich plates with application to underwater sound radiators", *J. Acoust. Soc. Am.*, 33, p. 1485 (1961).

[24] Hosaka, H., Itao, K. and Kuroda, S. "Damping characteristics of beam-shaped micro-oscillators", *Sensors Actuators A-Phys.*, 49, p. 87 (1995).

[25] Rankl, C., Pastushenko, V., Kienberger, F., Stroh, C.M. and Hinterdorfer, P. "Hydrodynamic damping of a magnetically oscillated cantilever close to a surface", *Ultramicroscopy*, 100, p. 301 (2004).

[26] Landau, L.D. and Lifshitz, E.M., *Fluid Mechanics*, Pergamon, London (1959).

[27] Korayem, M.H. and Ebrahimi, N. "Nonlinear dynamics of tapping-mode atomic force microscopy in liquid", *J. Appl. Phys.*, 109, p. 084301 (2011).

[28] Chon, W.M., Mulvaney, P. and Sader, J.E. "Experimental validation of theoretical models for the frequency response of atomic force microscope cantilever beams immersed in fluids", *J. Appl. Phys.*, 87, p. 8 (2000).

Moharam Habibnejad Korayem was born in Tehran, Iran, on April 21, 1961. He received his B.S. (Hon) and M.S. degrees in Mechanical Engineering from Amirkabir University of Technology in 1985 and 1987, respectively, and his Ph.D. degree in Mechanical Engineering from the University of Wollongong, Australia, in 1994. He is a Professor in Mechanical Engineering at Iran University of Science and Technology, where for the last 17 years, he has been involved with teaching and research activities in the area of robotics. His research interests include dynamics of elastic mechanical manipulators, trajectory optimization, symbolic modelling, robotic multimedia software, mobile robots, industrial robotics standard, robot vision, soccer robot, and the analysis of mechanical manipulators with maximum load carrying capacity. He has published more than 330 papers in international journals and conferences in his areas of interest.

Nazila Ebrahimi was born in Tehran, Iran, 1980. She received her B.S. degree in Mechanical Engineering from the University of Khajeh Nasir Toosi in 1998 and an M.S. degree in Automotive Engineering from Iran University of Science and Technology in 2005, where she is now a Ph.D. student. Her research interests include robotic systems, automotive engineering, atomic force microscopy dynamics, vibration and control and nanotechnology.

Mohammad Sadegh Sotoudegan was born in Shiraz, Iran 1988. He is currently a B.S. degree student at Iran University of Science and Technology. His research interests lie in the areas of micro/nano scale systems, microscopy techniques and robotics.